Applied Surface Science 360 (2016) 915–920

Contents lists available at ScienceDirect

Applied Surface Science

journal homepage: www.elsevier.com/locate/apsusc

Potential enhancement of antibacterial activity of graphene oxide-silver nanocomposite by introducing C_2 carbon chain linkage

Hyosuk Yun, Mohammad Shamsuddin Ahmed, Kyungmi Lee, Seungwon Jeon*, Chul Won Lee**

Department of Chemistry, Chonnam National University, Gwangju, 500-757, South Korea

ARTICLE INFO

Article history:
Received 28 May 2015
Received in revised form 21 October 2015
Accepted 8 November 2015
Available online 14 November 2015

Keywords:
Antibacterial materials
Carbon nanostructures
Grafted graphene
Silver nanoparticles

ABSTRACT

Various carbon chain linkages were introduced during the process of synthesizing silver-nanoparticles (AgNPs)-decorated graphene nanocomposites [referred to as GO-C_x-Ag where, HS-$(CH_2)_x$-SH = C_x and x = 0, 2, or 4] to evaluate antibacterial properties. The nano-structures of GO-C_x-Ag were characterized using TEM and XPS, revealing that GO-C_2-Ag comprises well-dispersed and smaller AgNPs anchored onto the surface of graphene sheets than the GO-C_0-Ag and GO-C_4-Ag. The antibacterial activities of those nanocomposites were assessed using paper-disk diffusion and minimal inhibitory concentration (MIC) methods against Gram-negative and Gram-positive bacteria. The results showed that carbon chain linkers enhanced the antibacterial activity against Gram-negative *Salmonella typhimurium* and *Pseudomonas aeruginosa* and Gram-positive *Staphylococcus aureus*. In particular, GO-C_2-Ag showed higher antibacterial activity than GO-C_0-Ag and GO-C_4-Ag due to nearly eight times higher reactive oxygen species (ROS) formation which determined by fluorescence-based ROS detection experiment. Also, LC-inductively coupled plasma mass spectrometer (LC-ICP-MS) demonstrated that the Ag release from GO-C_x-Ag was insignificant (0.03%). However, the higher ROS formation from GO-C_2-Ag was facilitated by higher dispersion, smaller size, and well attachment of AgNPs with AgO species onto graphene sheets. These results suggest that the medium length carbon chain linkers in between Ag and GO can be utilized to improve antibacterial activity.

1. Introduction

Many bacterial pathogens related to human disease have evolved into antibiotic-resistant microbes causing higher morbidity and mortality as these bacteria undergo multiple mutations [1]. This has become a grave and growing public health issue and, consequently, requires a new class of antibiotics to control multi-drug resistant microbes.

Silver nanoparticles (AgNPs) have emerged as antimicrobial agents due to their high surface area to volume ratio and distinctive physiochemical properties. AgNPs exhibit strong antimicrobial activity against both Gram-negative and Gram-positive bacteria including multi-drug resistant strains as well as pathogenic fungi [2,3]. Therefore, AgNPs are arising as new antibiotic agents, as they are comparable in efficacy and even more potent antimicrobial compounds than conventional antibiotics [4]. Furthermore, AgNPs have not been shown to cause resistance to antibiotic therapies, since AgNPs might exert their antibacterial effects through multiple targets, including bacterial walls, proteins, and DNA synthesis [3,5,6]. Currently, AgNPs are applicable as antibacterial and antifungal agents [7,8]. However, in spite of their potential antibiotic properties, AgNPs are highly reactive and easily susceptible to aggregation into large particles due to their high surface energy, resulting in a weakening of their unique chemical properties and a loss of their antimicrobial potencies. To solve these problems, various stable nanocomposites are composed of AgNPs dispersed on suitable substrates have been extensively studied [9–11]. Also, considering health hazards due to Ag increasing in environment, previous study suggests that the Ag as AgNPs is much safer than that of Ag^+ ion (Ag-salt) [12].

The carbon nanomaterials like graphene have unique electrical, physical, and chemical properties, which make it supportive candidate materials for various metal NPs such as AgNPs [13–16]. Studies on the preparation, characterization, and antibacterial activities of Ag nanocomposites have demonstrated that the antibacterial activities of Ag nanocomposites are dependent on the size, shape, and the degree of dispersion of AgNPs on the carbon nanostructures.

* Corresponding author. Tel.: +82 62 530 3380; fax: +82 62 530 3389.
** Corresponding author. Tel.: +82 62 530 3374; fax: +82 62 530 3389.
E-mail addresses: swjeon@chonnam.ac.kr (S. Jeon), cwlee@jnu.ac.kr (C.W. Lee).

http://dx.doi.org/10.1016/j.apsusc.2015.11.084
0169-4332/

Previous studies suggested that the thiolation is a simple and effective method for the preparation of metal-supported carbon materials including graphene; the samples exhibited excellent catalytic activity in various organic and electrochemical reactions [17–20] and antibacterial activities [21]. In particular, AgNP decorated CNT and graphene showed high and distinct antibacterial activities with minimal inhibitory concentration (MIC) values of 0.1–4 μg/mL against Gram-negative and Gram-positive bacteria [22], and they are reusable up to 20 cycles [21]. We also described the synthesis and catalytic activity of various carbon chain linkers grafted graphene oxide (GO) with AgNPs-decorated GO-S-$(CH_2)_x$-SH for oxygen reduction reaction (ORR) [23]. Of these, GO-C_2-Ag has the highest activity toward ORR. To expand our previous studies on the electrochemical properties of GO-C_x-Ag, we examined the antibacterial activities of the GO-C_x-Ag nanocomposites using paper-disk diffusion and MIC methods against Gram-negative and Gram-positive bacteria. The antimicrobial activities of GO-C_x-Ag nanocomposites depended on the length of carbon chain linkers. In particular, GO-C_2-Ag showed higher antibacterial activity against some selective Gram-negative and Gram-positive bacteria than GO-C_0-Ag and GO-C_4-Ag. LC-inductively coupled plasma mass spectrometer (LC-ICP-MS) and reactive oxygen species (ROS) detection experiments of GO-C_x-Ag nanocomposites revealed that the higher antibacterial activity of GO-C_2-Ag was induced by higher ROS formation. The instrumental analysis reveals that the higher ROS formation from GO-C_2-Ag could be influenced by higher dispersion, smaller size, and well attachment of AgNPs onto graphene sheets. These results indicate that the GO-C_2-Ag can be used to develop effective antibacterial nanomaterials.

2. Materials and methods

2.1. Preparation of the antibacterial materials

2.1.1. Chemicals and reagents

The graphite powder (~325 mesh, 99.999%), tetrahydrofuran (THF), ethanol, 1,2-ethanedithiol [HS-$(CH_2)_2$-HS; C_2], and 1,4-butanedithiol [HS-$(CH_2)_4$-HS; C_4] were obtained from Sigma-Aldrich. $KMnO_4$, H_2SO_4, and H_3PO_4 were purchased from Dae-jung Co., Korea. $AgNO_3$ was purchased from Ducksan Pure Chemical Industries Co., Ltd. The membrane filters (pore size: 0.2 μm and diameter: 47 mm; and pore size: 1.0 μm and diameter: 47 mm) were purchased from Millipore Corporation in Bedford and Whatman. Other reagents were of analytical grade and were used as received without further purification.

2.1.2. Synthesis of GO-C_x-Ag

GO was prepared by oxidizing graphite using the improved Hummers method [24–27]. The GO-C_x-SH was obtained using a modified method [27]. Briefly, the GO and the linker materials, HS-$(CH_2)_x$-SH (where $x = 0, 2, 4$), were separately dispersed with tetrahydrofuran (THF) into four round-bottom flasks and stirred at 55 °C for 20 h followed by 30 min ultrasonic agitation. The samples were separated from the mixture using filtration, washed several times with THF, methanol, ethanol, and distilled water (DW), and dried in a vacuum oven at 50 °C for 18 h. The GO-C_x-Ag mixture was prepared by adding 50 mg of GO-C_x-SH to 15 mL of DW for 30 min with ultrasonic agitation. Then 0.1 M $AgNO_3$ (5 mL) and 0.1 M NaOH (2 mL) were added to the mixture and stirred for 20 h. The GO-C_x-Ag products were obtained *via* centrifugation, washed with DW, and vacuum-dried for 24 h at 50 °C.

2.2. Characterization of GO-C_x-Ag

X-ray photoelectron spectroscopy (XPS) was performed with a VG Multilab 2000 spectrometer (Thermo VGScientific, South-end-on-Sea, Essex, UK) using an ultra-high vacuum. The XPS data analysis program Avantage version 4.54 (Thermo Electron Corp., England) was used. This system uses an unmonochromatized Mg K (1253.6 eV) source and a spherical section analyzer. Survey scan data were collected using 50 eV pass energy. The transmission electron microscopy (TEM) images and energy dispersive X-ray spectroscopy (EDX) were carried out on a copper grid with a TECNAI 20 microscope at 200 kV.

2.3. Evaluation of antimicrobial activity

2.3.1. Paper-disk diffusion method

The paper-disc diffusion method was used to determine the antibacterial activities of the samples. Bacteria were initially cultured with Luria-Bertani (LB) media at 37 °C for 12 h. A suspension of *Escherichia coli* (KCTC 1682) and *Staphylococcus aureus* (KCTC 1621) [50 μL with 1×10^7 colony forming units/mL (CFU/mL)], which were obtained from the Korean Collection for Type Cultures (KCTC) at the Korea Research Institute of Bioscience and Biotechnology, were inoculated into Mueller Hinton agar (MHA) plates. Whatman filter paper discs (4 mm diameter) were placed on the inoculated plates, and 20 μL of 16 μg/mL samples were added and allowed to dry for 15 min, after which they were incubated at 37 °C for 24 h.

2.3.2. MIC measurements

The antibacterial activities of the GO-Ag nanocomposites were tested in sterile 96-well 200 μL plates as follows. Aliquots (100 μL) of the cell suspension at 4×10^6 CFU/mL in 1% peptone were added to 100 μL of the sample solutions (serial two-fold dilutions in 1% peptone). After incubation for 16 h at 37 °C, the MIC was determined by visual examination on the basis of the lowest concentration of sample solution in cells with no bacterial growth. Three Gram-negative bacteria (*E. coli* [KCTC 1682], *Salmonella typhimurium* [KCTC 1926], and *Pseudomonas aeruginosa* [KCTC 1637]) and three Gram-positive bacteria (*Bacillus subtilis* [KCTC 3068], *Staphylococcus epidermidis* [KCTC 1917], and *S. aureus* [KCTC 1621]) were procured from the KCTC at the Korea Research Institute of Bioscience and Biotechnology.

2.4. Detection of Ag and ROS

The amount of Ag released from the GO-Ag nanocomposites was determined by LC-ICP-MS using a Nexion model 300X (Perkin Elmer). ROS formation from GO-C_x-Ag nanocomposites was determined using 2′7′-dichlorofluorescein diacetate (DCFDA) [28,29]. The GO-silver nanomaterials (30 μg/mL) were incubated in distilled water at 37 °C for 3 h and centrifuged at 4 °C for 5 min at 21,400 × *g* to remove insoluble materials. The supernatant was treated with 1 μM DCFDA for 1 h. ROS formation was detected using a fluorescence excitation wavelength of 502 nm and an emission wavelength of 523 nm using a fluorescence spectrophotometer (Hitachi F-4500).

3. Results and discussion

Scheme 1 shows that the linker molecules are first bonded through –SH with the GO (–COOH) *via* condensation reaction and produce a –C–S bond. It is, however, another $-S^-$ at upper side is now free to attach Ag^+ *via* negative-positive charge interaction, respectively. Finally, the AgNPs have been formed by alkaline treatment.

The surface morphologies of GO-C_x-Ag (where $x = 0, 2$, or 4) were characterized using TEM. Fig. 1 includes TEM images of GO-C_x-Ag and shows the presence of a large number of AgNPs on the surface of

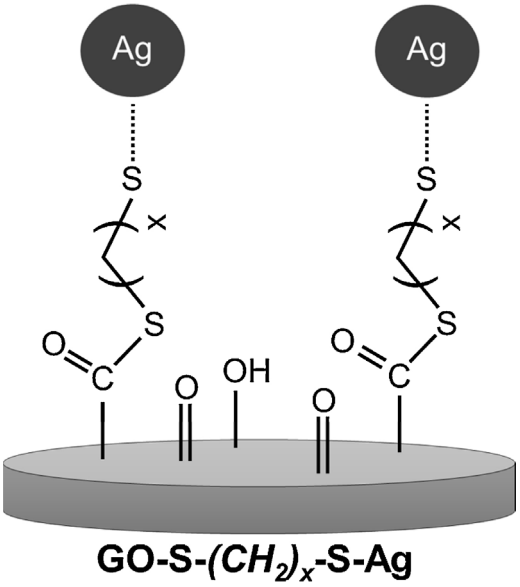

Scheme 1. The schematic diagram of the synthesis process of the GO-C_x-Ag (where $x = 0$, 2, or 4).

GO. For GO-C_0-Ag, various sizes of AgNPs were anchored to the surface of GO (Fig. 1a). Some agglomerations of AgNPs were observed, which yielded a larger size distribution and displayed irregularly sizes of AgNPs. For GO-C_2-Ag and GO-C_4-Ag, smaller and evenly sizes of AgNPs appeared on the surface (Fig. 1b and c). In particular, for GO-C_2-Ag, smaller and quasi-spherical AgNPs were uniformly dispersed on the GO surface (Fig. 1b). Most of the AgNP's diameter was in the range of 2–4 nm and average 2.8 ± 0.1 nm (Fig. 2a). On the other hand, the average size of AgNPs for GO-C_4-Ag was 7.6 ± 1.1 nm (Fig. 2b), which is larger than that of AgNPs in GO-C_2-Ag. The corresponding EDX spectra also suggest that the AgNPs have anchored onto the GO *via* linker molecules while distinguishable signals were from C, O, S, Ag and Cu (Cu peak was attributable to the TEM copper grid) with no other contaminant elements (Fig. 1d). The GO-C_x-Ag nanocomposites were further characterized using XPS (Fig. 3) [23]. In brief, the XPS survey spectra for GO-C_x-Ag show the C1s (284 eV), O1s (532 eV), Ag3d (367 eV), and S2p (162 eV) peaks. The core level of C1s of XPS spectra showed that the C–O bond of GO-C_2-Ag is much higher than that of GO-C_4-Ag and GO-C_0-Ag due to influence of C–S over C–O bond (Fig. 3a) [30], suggesting the higher degree of carbon chain linker attachment in GO-C_2-Ag than GO-C_4-Ag. Also, high-resolution S2p spectra revealed that higher amount of S was detected in GO-C_2-Ag than GO-C_4-Ag, indicating that the higher amount of SH-C_2-SH molecules were attached onto GO while both linker's molecules have same S atom (Fig. 3b). The higher reactivity of SH-C_2-SH than SH-C_4-SH results from the lower hydrophobic behavior of SH-C_2-SH than SH-C_4-SH, since higher C-content molecules have lower solubility in water (such as, graphene and hydrocarbon). Furthermore, the lower flexibility of SH-C_2-SH than SH-C_4-SH may enhance the homogeneous grafting of SH-C_2-SH onto GO. The Ag peaks at $Ag3d_{5/2}$ and $Ag3d_{3/2}$ correspond to 368.91 and 375.03 eV, 367.93 and 373.92 eV, and 368.59 and 374.59 eV for GO-C_0-Ag, GO-C_2-Ag, and GO-C_4-Ag, respectively.

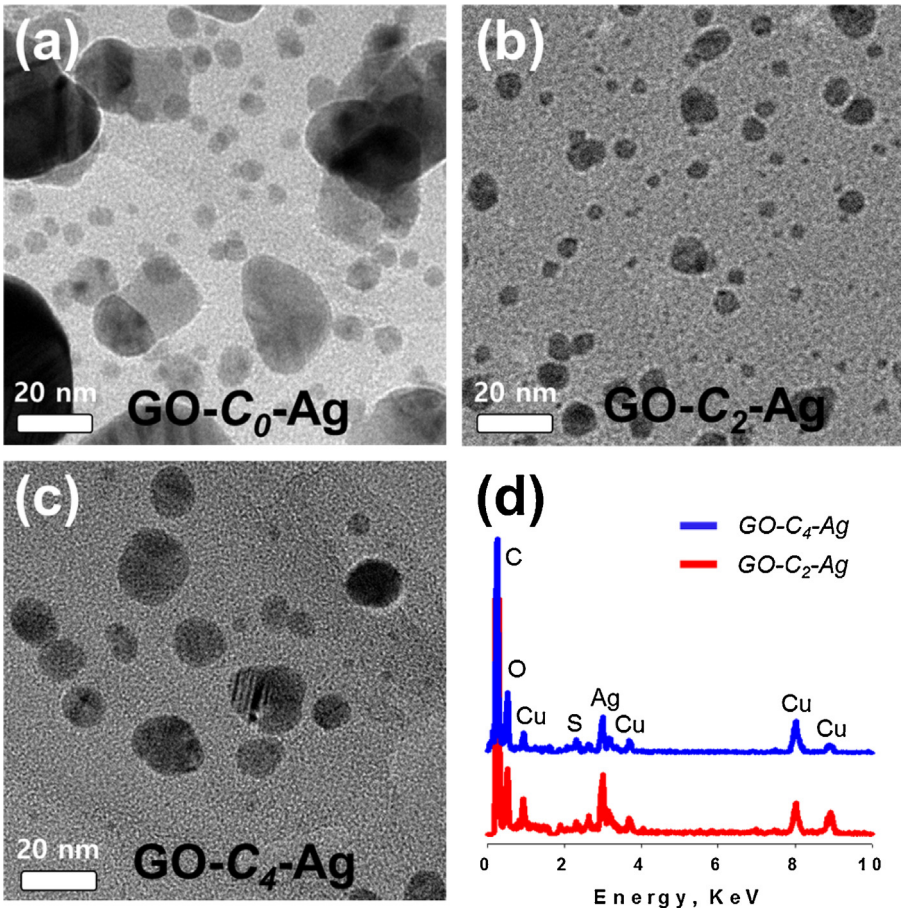

Fig. 1. TEM images of the all GO-C_x-Ag nanocomposites (a–c), and EDX spectra of GO-C_2-Ag and GO-C_4-Ag (d).

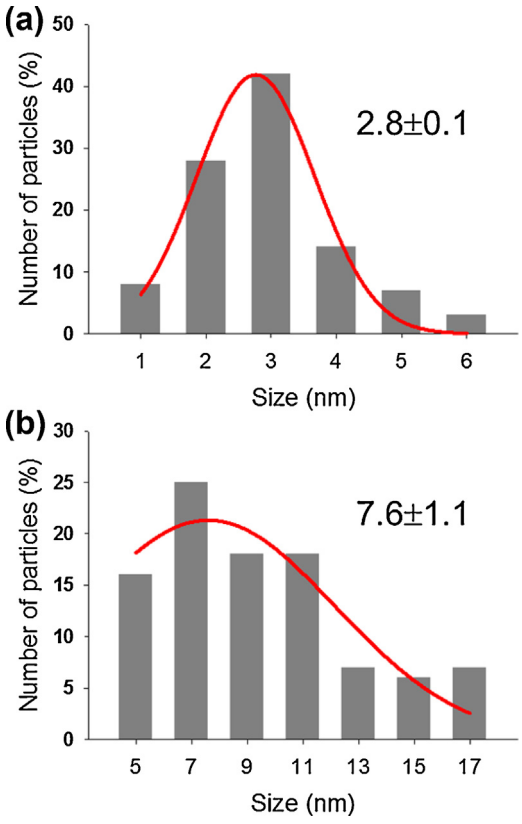

Fig. 2. The size distribution of GO-C_2-Ag (a) and GO-C_4-Ag (b) was calculated from the TEM images (Fig. 1).

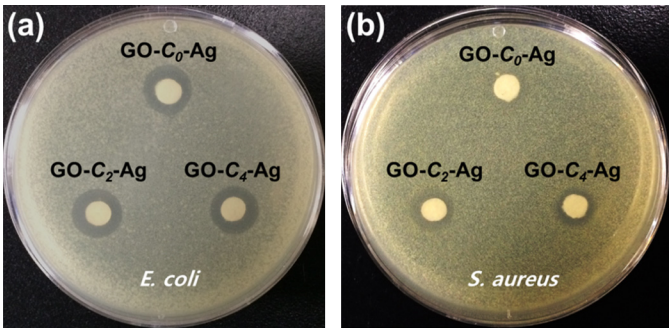

Fig. 4. Photographs of the antibacterial test results using the paper-disk diffusion method against Gram-negative *E. coli* (a) and Gram-positive *S. aureus* (b).

These are consistent with the expected spin energy difference of approximately ~6 eV. The higher binding energy shift was observed in GO-C_2-Ag and this value is typical for AgO (Fig. 3c) [31].

The antibacterial activities of the GO-C_x-Ag nanocomposites were initially assessed using a paper-disk diffusion method for Gram-negative *E. coli* and Gram-positive *S. aureus* bacteria. As shown in Fig. 4a, all GO-C_x-Ag nanocomposites formed similarly size of inhibition zones against *E. coli*, indicating similar antibacterial effects. However, the level of inhibitory effect on *S. aureus* was not similar among all different GO-C_x-Ag nanocomposites (Fig. 4b). The inhibitory effect for GO-C_0-Ag was much weaker (no inhibitory zone) than those of GO-C_2-Ag and GO-C_4-Ag. Furthermore, the inhibition zone for GO-C_2-Ag was slightly larger than that of GO-C_4-Ag (diameter of 12 mm versus 9 mm). These data suggest that the GO-C_2-Ag nanocomposite exhibits distinct antibacterial activities against different bacterial species. Thus, to quantitatively assess antibacterial activities, we measured the MIC values of the

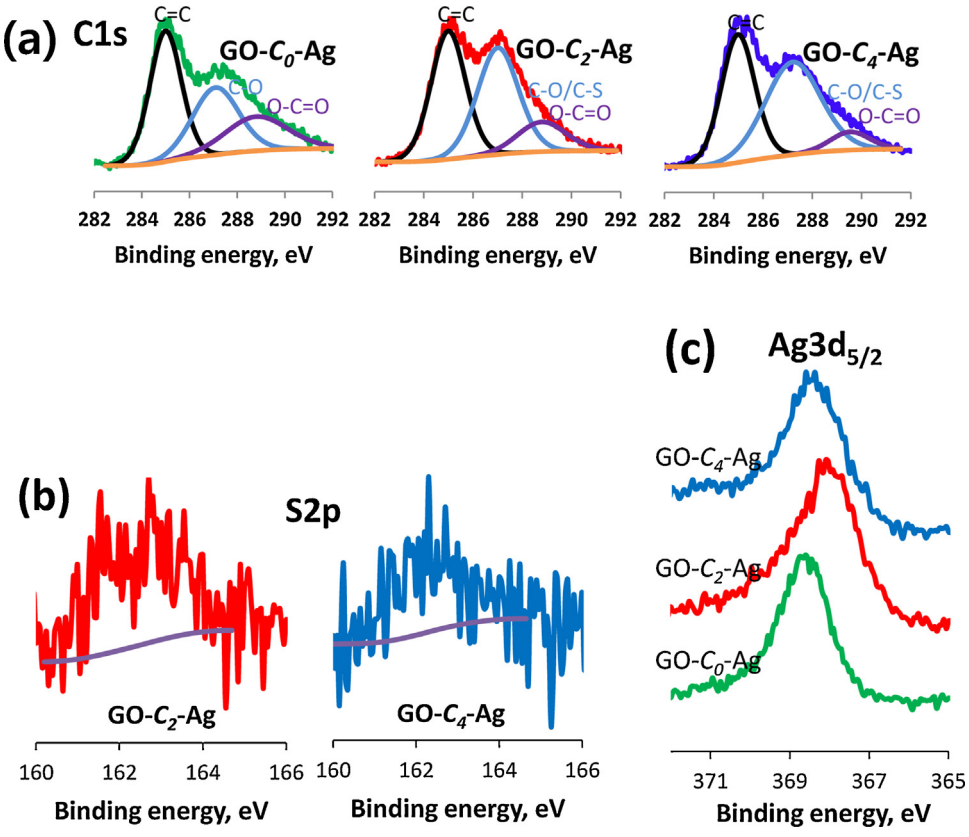

Fig. 3. The core level of C1s (a), S2p (b) and Ag3d$_{5/2}$ (c) XPS spectra of GO-C_x-Ag.

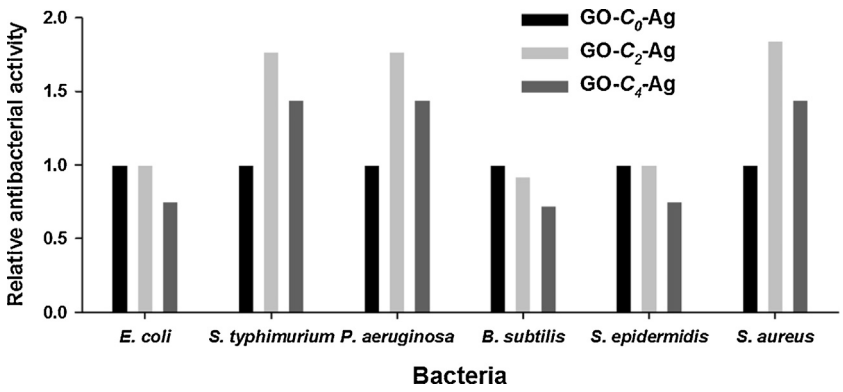

Fig. 5. The relative antibacterial activities of GO-C_0-Ag, GO-C_2-Ag, and GO-C_4-Ag against Gram-negative *E. coli*, *S. typhimurium*, and *P. aeruginosa* and Gram-positive *B. subtilis*, *S. epidermidis*, and *S. aureus*.

Table 1
Summary of minimal inhibitory concentration (μg/mL) against Gram-negative and Gram-positive bacteria.

Bacteria	GO-C_0-Ag	GO-C_2-Ag	GO-C_4-Ag
Gram (−)			
E. coli	0.6	0.6	0.8
S. typhimurium	2.3	1.3	1.6
P. aeruginosa	2.3	1.3	1.6
Gram (+)			
B. subtilis	2.3	2.5	3.2
S. epidermidis	0.6	0.6	0.8
S. aureus	4.6	2.5	3.2

all GO-C_x-Ag nanocomposites against three Gram-negative and three Gram-positive bacteria (Table 1). The MIC value for GO-C_0-Ag against *E. coli* and *S. epidermidis* is 0.6 μg/mL, which is much lower than those of other bacteria (in the range of 2.3–4.6 μg/mL). These data suggest that *E. coli* and *S. epidermidis* were more susceptible to the GO-C_0-Ag nanocomposite than other bacteria. To examine the antibacterial effects of various carbon chain linkages of GO-C_x-Ag nanocomposites, we also measured the MIC values (Table 1) and summarized their relative antibacterial activities based on these values (Fig. 5). Interestingly, the carbon chain linker containing nanocomposites (GO-C_2-Ag and GO-C_4-Ag) exhibited enhanced antibacterial activities against *S. typhimurium*, *P. aeruginosa*, and *S. aureus*. In particular, the GO-C_2-Ag had enhanced antibacterial activity up to 1.8 times compared with GO-C_0-Ag (Fig. 5). The insertion of carbon chain linkers between GO and AgNP did not show any enhanced antibacterial activities against *E. coli*, *B. subtilis*, and *S. epidermidis*. Although the antibacterial activities against different bacterial species are appearing to vary due to the microorganism varies by the types and structural features, these results indicate that there are distinct antibacterial susceptibilities among bacterial species to the GO-C_2-Ag nanocomposites.

The antibacterial mechanism of AgNPs is at least partially understood. AgNPs might attack the bacterial membrane, leading to a change in the permeability of the membranes, leakage of reducing sugars and proteins, and inactivation of respiratory chain dehydrogenases [32,33]. Since the antibacterial activities of GO-C_2-Ag and GO-C_4-Ag nanocomposites were mainly due to the adhered AgNPs but not GO itself [21], we determined the amount of Ag released from the GO-C_x-Ag nanocomposites using LC-ICP-MS. The results showed that a very small amount of Ag dissolution (less than 0.03% of the total Ag) was detected from the GO-C_x-Ag nanocomposites (Table 2), indicating that the dissolved Ag cannot affect the bactericidal activity. It is, however, recent studies have demonstrated that the antibacterial activity of AgNPs is related to ROS

Table 2
Amount of dissolved Ag released from GO-C_x-Ag nanocomposites.

GO-silver nanocomposites	Ag (μg/mL)	Ag (%)[a]
GO-C_0-Ag	<0.15	<0.03
GO-C_2-Ag	<0.15	<0.03
GO-C_4-Ag	<0.15	<0.03

[a] Percentage of Ag released from the total Ag (600 μg/mL) attached to GO-C_x-Ag.

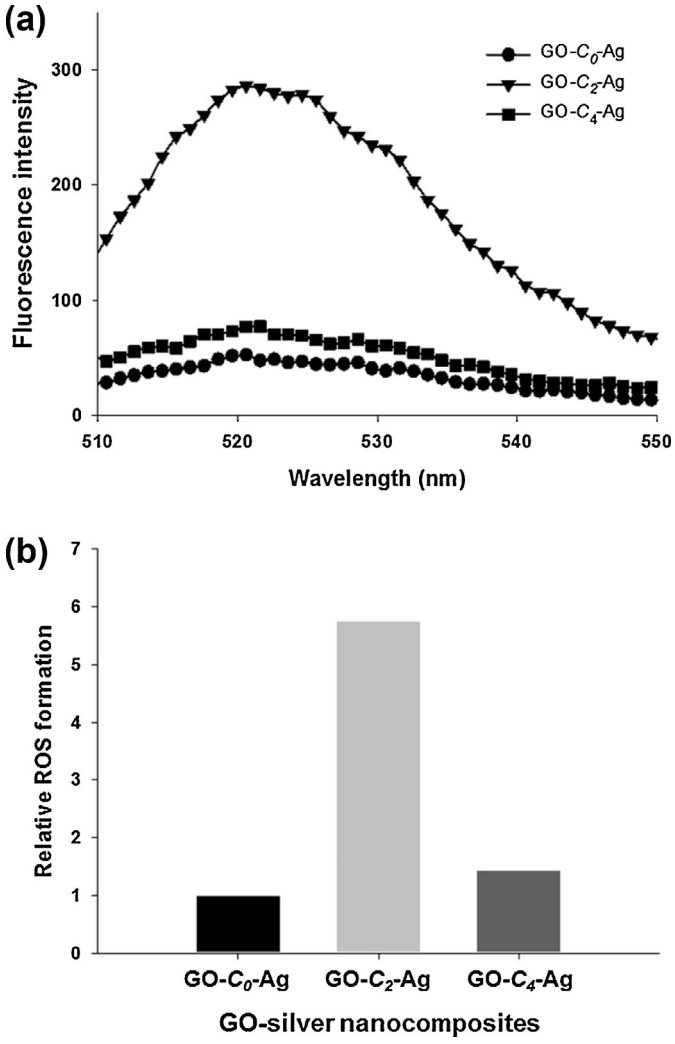

Fig. 6. Fluorescence spectra of DCFDA induced by GO-C_x-Ag (a) and relative ROS formation converted from the GO-C_x-Ag induced fluorescence intensity at 523 nm (b).

formation, which can attack the outer bacterial membrane or peptidoglycan layer and then induce irregular fragmentation of the bacterial cells [34]. Thus, we measured ROS production using ROS induced fluorescence of DCFDA since DCFDA fluorescence can be increased with the increasing of ROS [29]. Fig. 6a shows the fluorescence spectra of DCFDA induced by GO-C_x-Ag. The GO-C_2-Ag induced fluorescence was greatly higher compared to GO-C_0-Ag and GO-C_4-Ag, indicating that the GO-C_2-Ag produces much more ROS than the others. In addition, higher AgO species was found in GO-C_2-Ag by XPS analysis. Also, Fig. 6b shows the relative ROS formation converted from the GO-C_x-Ag induced fluorescence intensity at 523 nm. Interestingly, the relative ROS formation by GO-C_2-Ag is much larger than the others. Among all the GO-C_x-Ag nanocomposites, the GO-C_2-Ag showed the highest antibacterial activity, likely due to higher ROS formation. Our previous studies using GO-C_x-Ag revealed that GO-C_2-Ag had a better activity toward ORR than that of GO-C_0-Ag and GO-C_4-Ag [23]. Taken together, the enhanced antibacterial and electrocatalytic activities of GO-C_2-Ag might be the result of an increased grafting of linker molecules and a smaller size of AgNPs on the GO sheets.

4. Conclusions

The effect of the carbon chain linker in between AgNPs and GO (GO-C_x-Ag) nanocomposite was evaluated for antibacterial activity against Gram-negative and Gram-positive bacteria. TEM and XPS analyses of GO-C_2-Ag revealed that smaller sized AgNPs were well-dispersed onto the surface of graphene sheets compared to the GO-C_0-Ag and GO-C_4-Ag. To determine the antibacterial activity, paper-disk diffusion and MIC methods were used for the GO-C_x-Ag nanocomposites, which indicated the carbon chain linkers enhanced the antibacterial activity against some selective Gram-negative *S. typhimurium* and *P. aeruginosa* and Gram-positive *S. aureus*. The antibacterial activity of GO-C_2-Ag was higher than those of GO-C_0-Ag and GO-C_4-Ag. The LC-ICP-MS and ROS detection experiments suggested that the enhancement of the antibacterial activity of GO-C_2-Ag was induced by ROS formation, which might result from the well-dispersed and smaller AgNPs with AgO species onto the surface of GO.

Acknowledgments

This work was supported by the Basic Science Research Program through the National Research Foundation of Korea (NRF) funded by the Ministry of Education, Science, and Technology of Korea (NRF-2013R1A1A2009419 to C.W.L).

References

[1] J. Davies, D. Davies, Origins and evolution of antibiotic resistance, Microbiol. Mol. Biol. R 74 (2010) 417–433.
[2] A. Panacek, L. Kvitek, R. Prucek, M. Kolar, R. Vecerova, N. Pizurova, V.K. Sharma, T. Nevecna, R. Zboril, Silver colloid nanoparticles: synthesis, characterization, and their antibacterial activity, J. Phys. Chem. B 110 (2006) 16248–16253.
[3] J.R. Morones, J.L. Elechiguerra, A. Camacho, K. Holt, J.B. Kouri, J.T. Ramirez, M.J. Yacaman, The bactericidal effect of silver nanoparticles, Nanotechnology 16 (2005) 2346–2353.
[4] R. Roy, M.R. Hoover, A.S. Bhalla, T. Slawecki, S. Dey, W. Cao, J. Li, S. Bhaskar, Ultradilute Ag-aquasols with extraordinary bactericidal properties: role of the system Ag-O-H2O, Mater. Res. Innov. 11 (2007) 3–18.
[5] S. Shrivastava, T. Bera, A. Roy, G. Singh, P. Ramachandrarao, D. Dash, Characterization of enhanced antibacterial effects of novel silver nanoparticles, Nanotechnology 18 (2007).
[6] S.K. Gogoi, P. Gopinath, A. Paul, A. Ramesh, S.S. Ghosh, A. Chattopadhyay, Green fluorescent protein-expressing *Escherichia coli* as a model system for investigating the antimicrobial activities of silver nanoparticles, Langmuir 22 (2006) 9322–9328.
[7] J.T. Seil, T.J. Webster, Antimicrobial applications of nanotechnology: methods and literature, Int. J. Nanomed. 7 (2012) 2767–2781.
[8] M.J. Hajipour, K.M. Fromm, A.A. Ashkarran, D.J. de Aberasturi, I.R. de Larramendi, T. Rojo, V. Serpooshan, W.J. Parak, M. Mahmoudi, Antibacterial properties of nanoparticles, Trends Biotechnol. 30 (2012) 499–511.
[9] X.L. Cao, M. Tang, F. Liu, Y.Y. Nie, C.S. Zhao, Immobilization of silver nanoparticles onto sulfonated polyethersulfone membranes as antibacterial materials, Colloid Surf. B 81 (2010) 555–562.
[10] T. Angelova, N. Rangelova, R. Yuryev, N. Georgieva, R. Muller, Antibacterial activity of SiO2/hydroxypropyl cellulose hybrid materials containing silver nanoparticles, Mat. Sci. Eng. C-Mater. 32 (2012) 1241–1246.
[11] B. Roy, P. Bharali, B.K. Konwar, N. Karak, Silver-embedded modified hyperbranched epoxy/clay nanocomposites as antibacterial materials, Bioresource Technol. 127 (2013) 175–180.
[12] M. van der Zande, R.J. Vandebriel, E.V. Doren, E. Kramer, Z.H. Rivera, C.S. Serrano-Rojero, E.R. Gremmer, J. Mast, R.J.B. Peters, P.C.H. Hollman, P.J.M. Hendriksen, H.J.P. Marvin, A.A.C.M. Peijnenburg, H. Bouwmeester, Distribution, elimination, and toxicity of silver nanoparticles and silver ions in rats after 28-day oral exposure, ACS Nano 6 (2012) 7427–7442.
[13] K.S. Novoselov, A.K. Geim, S.V. Morozov, D. Jiang, Y. Zhang, S.V. Dubonos, I.V. Grigorieva, A.A. Firsov, Electric field effect in atomically thin carbon films, Science 306 (2004) 666–669.
[14] M.S. Ahmed, S. Jeon, Electrochemical activity evaluation of chemically damaged carbon nanotube with palladium nanoparticles for ethanol oxidation, J. Power Sources 282 (2015) 479–488.
[15] J.E. Choe, M.S. Ahmed, S. Jeon, 3,4-Ethylenedioxythiophene functionalized graphene with palladium nanoparticles for enhanced electrocatalytic oxygen reduction reaction, J. Power Sources 281 (2015) 211–218.
[16] M.S. Ahmed, H.S. Han, S. Jeon, One-step chemical reduction of graphene oxide with oligothiophene for improved electrocatalytic oxygen reduction reactions, Carbon 61 (2013) 164–172.
[17] M.S. Ahmed, D. Kim, H.S. Han, H. Jeong, S. Jeon, Covalent hybridization of thiolated graphene sheet and platinum nanoparticles for electrocatalytic oxygen reduction reaction, J. Nanosci. Nanotechnol. 12 (2012) 8349–8355.
[18] K. Lee, M.S. Ahmed, S. Jeon, Electrochemical deposition of silver on manganese dioxide coated reduced graphene oxide for enhanced oxygen reduction reaction, J. Power Sources 288 (2015) 261–269.
[19] M.S. Ahmed, D. Kim, S. Jeon, Covalently grafted platinum nanoparticles to multi walled carbon nanotubes for enhanced electrocatalytic oxygen reduction, Electrochim. Acta 92 (2013) 168–175.
[20] M. Yun, M.S. Ahmed, S. Jeon, Thiolated graphene oxide-supported palladium cobalt alloyed nanoparticles as high performance electrocatalyst for oxygen reduction reaction, J. Power Sources 293 (2015) 380–387.
[21] J.D. Kim, H. Yun, G.C. Kim, C.W. Lee, H.C. Choi, Antibacterial activity and reusability of CNT-Ag and GO-Ag nanocomposites, Appl. Surf. Sci. 283 (2013) 227–233.
[22] H. Yun, J.D. Kim, H.C. Choi, C.W. Lee, Antibacterial activity of CNT-Ag and GO-Ag nanocomposites against gram-negative and gram-positive bacteria, Bull. Korean Chem. Soc. 34 (2013) 3261–3264.
[23] K. Lee, M.S. Ahmed, S. Jeon, Various carbon chain containing linkages grafted graphene with silver nanoparticles electrocatalysts for oxygen reduction reaction, J. Electrochem. Soc. 162 (2015) F1–F8.
[24] M.S. Ahmed, S. Jeon, Highly active graphene-supported Ni_xPd_{100-x} binary alloyed catalysts for electro-oxidation of ethanol in an alkaline media, ACS Catal. 4 (2014) 1830–1837.
[25] M.S. Ahmed, J.M. You, H.S. Han, D.C. Jeong, S. Jeon, A green preparation of nitrogen doped graphene using urine for oxygen reduction in alkaline fuel cells, J. Nanosci. Nanotechno. 14 (2014) 5722–5729.
[26] D.C. Marcano, D.V. Kosynkin, J.M. Berlin, A. Sinitskii, Z.Z. Sun, A. Slesarev, L.B. Alemany, W. Lu, J.M. Tour, Improved synthesis of graphene oxide, ACS Nano 4 (2010) 4806–4814.
[27] D. Kim, M.S. Ahmed, S. Jeon, Different length linkages of graphene modified with metal nanoparticles for oxygen reduction in acidic media, J. Mater. Chem. 22 (2012) 16353–16360.
[28] H. Ischiropoulos, A. Gow, S.R. Thom, N.W. Kooy, J.A. Royall, J.P. Crow, Detection of reactive nitrogen species using 2,7-dichlorodihydrofluorescein and dihydrorhodamine 123, Method Enzymol. 301 (1999) 367–373.
[29] J.P. Crow, Dichlorodihydrofluorescein and dihydrorhodamine 123 are sensitive indicators of peroxynitrite in vitro: implications for intracellular measurement of reactive nitrogen and oxygen species, Nitric Oxide 1 (1997) 145–157.
[30] M.S. Ahmed, S. Jeon, New functionalized graphene sheets for enhanced oxygen reduction as metal-free cathode electrocatalysts, J. Power Sources 218 (2012) 168–173.
[31] Z.-H. Yang, C.-H. Ho, S. Lee, Plasma-induced formation of flower-like Ag_2O nanostructures, Appl. Surf. Sci. 349 (2015) 609–614.
[32] W.K. Jung, H.C. Koo, K.W. Kim, S. Shin, S.H. Kim, Y.H. Park, Antibacterial activity and mechanism of action of the silver ion in Staphylococcus aureus and Escherichia coli, Appl. Environ. Microb. 74 (2008) 2171–2178.
[33] Q.L. Feng, J. Wu, G.Q. Chen, F.Z. Cui, T.N. Kim, J.O. Kim, A mechanistic study of the antibacterial effect of silver ions on escherichia coli and staphylococcus aureus, J. Biomed. Mater. Res. 52 (2000) 662–668.
[34] C. Pellieux, A. Dewilde, C. Pierlot, J.M. Aubry, Bactericidal and virucidal activities of singlet oxygen generated by thermolysis of naphthalene endoperoxides, Method Enzymol. 319 (2000) 197–207.